Earth System
Science
Data

Open Access

Discussions

Wind waves in the North Atlantic from ship navigational radar: SeaVision development and its validation with Spotter wave buoy and WaveWatch III

5   Natalia Tilinina[1,2], Dmitry Ivonin[1], Alexander Gavrikov[1], Vitaly Sharmar[1], Sergey Gulev[1,3], Alexander Suslov[1], Vladimir Fadeev[4], Boris Trofimov[4], Sergey Bargman[4], Leysan Salavatova[5], Vasilisa Koshkina[5], Polina Shishkova[1], Olga Razorenova[1] and Alexey Sokov[1]

[1] Shirshov Institute of Oceanology, RAS, Nakhimovsky ave. 36, 117997, Moscow, Russia
10 [2] Université Grenoble Alpes, IGE, 70 rue de la Physique, 38400, Grenoble, France
[3] A.M. Obukhov Institute of Atmospheric Physics, RAS, 3, Pyzhevskiy Lane, Moscow, 109017, Russia
[4] Joint stock company "Marine Complexes and Systems", 13th line of Vasilyevsky Island, 199034, Saint Petersburg, Russia.
[5] Moscow Institute of Physics and Technology, Institutskiy Pereulok 9, 141701, Dolgoprudny, Moscow Region, Russia

Correspondence to: Natalia Tilinina (tilinina@sail.msk.ru) and Alexander Gavrikov (gavr@sail.msk.ru)

15 **Abstract**

The global coverage of the observational network of the wind waves is still characterized by the significant gaps in *in situ* observations. At the same time wind waves play an important role into the Earth' climate system specifically in the air-sea interaction processes and energy exchange between the ocean and the atmosphere. In this paper we present the SeaVision system for measuring wind waves' parameters in the open ocean with navigational marine X-band radar and prime data
20 collection from the three research cruises in the North Atlantic (2020 and 2021) and Arctic (2021). Simultaneously with SeaVision observations of the wind waves we were collecting data in the same locations and time with Spotter wave buoy and running WaveWatch III model over our domains. Measurements with SeaVision were quality controlled and validated by comparison with Spotter buoy data and WaveWatch III experiments. Observations of the wind waves with navigational X-band radar are in agreement among these three sources of data, with the best agreement for wave propagation directions. The
25 dataset that supports this paper consists of significant wave height, wave period and wave energy frequency spectrum from both SeaVision and Spotter buoy. Currently the dataset is available through the temporary link (https://sail.ocean.ru/tilinina2021/) while supporting dataset (Tilinina et al., 2021) is in technical processing at PANGAEA repository. The dataset can be used for validation of satellite missions as well as model outputs. One of the major highlights in this study is potential of all ships navigating into the open ocean and equipped with X-band marine radar to participate into
30 the development of another observational network for the wind waves in the open ocean once cheap and independently operating version of the SeaVision (or any other system) is available.

Earth System
Open Access
Science
Data
Discussions

1 Introduction

The history of wind waves studies in the ocean demonstrated a critically important role of the wind waves into the climate system, specifically in air-sea interaction processes and energy exchange between the ocean and the atmosphere. At the same
35   time, the history of building a robust global and regional datasets for assessment of the wind waves climatology and dynamics revealed that the wave fields are always hard to measure both remotely and in situ with sufficient temporal and spatial resolutions to cover global and regional domains (comparing with e.g. air temperature or sea surface temperature).

Regular observations of the wind waves date back to the 19th century when the Voluntary Observing Ships (VOS) reported first visual observations of wind waves in the open ocean. However, the VOS dataset is characterized by sparse spatial and
40   temporal resolutions and by the bias of the individual observers – marine officers.

Remote sensing datasets of the wind waves are dating back to 1985 (Ribal and Young, 2019), when the first satellite radar altimeters missions began measurements of the elevations of the ocean surface, providing better temporal and spatial cover of wind waves fields. At the same time remote sensing has to be validated with *in situ* measurements, typically buoys that are deployed in coastal regions (such as NDBC buoys, Swail et al. 2010 or NOWPHAS, Nagai et al. 2005). Buoys are measuring
45   vertical and horizontal displacements of the ocean surface (such as Spotter or Datawell buoys with up to 2.5 Hz sampling frequency, Raghukumar et al., 2019) and are the most precise and effective way to estimate wind waves characteristics, providing accurate inputs for the data assimilation in Numerical Weather Prediction (NWP) models and theoretical studies. Being very important and accurate data providers, buoys cover only a few locations and rather can be used as "ground truth" for verification of all other dataset.

50   Significant improvement of the global picture of the wind waves is dating back to 1988 when the obvious relation between the wind and waves was implemented in spectral wave models as Discrete Interaction Approximation (DIA) parametrization (WAMDI, 1988; Hasselman et al., 1985; Cavaleri et al., 2020), while first relations between wind and waves were quantified by (Sverdrup and Munk, 1947). Nowadays wave modelling is suffering from the lack of accuracy for modelling and prediction of extremely high wave peaks during high wind speeds (e.g. during the storm passage, Cavaleri et al., 2020).

55   An important operational task is delivery of the wave forecast to the ships in the open ocean, which is typically (i) not very operational and (ii) not very accurate during the rough sea conditions. Thus, within this paper we present results of development and validation of the SeaVision system for (i) collecting wind waves observations in the open ocean using navigational marine X-band radar and (ii) to monitor in real time wave heights, direction and period along the ship track in the open ocean.

The methodology of the navigational marine radar adaptation for measurements of the wind waves characteristics was
60   announced by (Young et al., 1985). The radar images of the ocean surface, known as sea clutter, are generated by the Bragg scattering (Crombie, 1955) of the electromagnetic signal by the ripples on the ocean surface produced by the wind. Being emitted from the radar, an electromagnetic signal reaches the ocean surface and further, being reflected by ripples on the ocean surface, received back by the radar antenna when the ocean surface is rough enough (i.e. ripples are developed). Under conditions of the wind speed > 3 m/s and waves height > 0.5 m waves field becomes visible on the radar image of the sea

65   clutter (Hatten et al., 1998; Hessner and Hanson, 2010). Time sequences of these images are further analyzed in space and time for estimation of wind waves' characteristics. Using various approaches: signal-to-noise ratio derived from the image spectrum (Nieto-Borge et al., 1999; Neito-Borge et al., 2008; Seemann et al., 1997), statistical analysis of island-to-trough ratio on the sea clutter images (Buckley and Alter, 1997; Buckley and Alter, 1998), analysis of the images' texture (Gangeskar, 2000), wavelet technique (Huang and Gill, 2015), the least square approach (Huang et al., 2014) and shadowing analysis

70   (Gangeskar, 2014; Liu et al., 2015), or combination of these methods with usage of artificial neural networks (Vicen-Bueno et al., 2012), analysis of the Doppler shift of the received radar signal because of the well-defined relationship between orbital velocities and wave height for linear gravity waves (Plant, 1997; Plant et al., 1987; Johnson et al., 2009; Hwang et al., 2010; Hackett et al., 2011; Chen et al., 2019). There are many aspects of the sea clutter radar images analysis, for example (Nieto Borge and Guedes Soares, 2000) proposed an approach for analysis of the sea states consisting of superpositions of swell and

75   wind sea components, that allows to derive wind waves and swell contributions to the total wave field, together with directional characteristic of the wave field.

There are also examples and techniques for using images of the sea clutter from X-band radars for estimation of the current-depth profiles with Eulerian approach (Campana et al., 2017), to retrieve wind speed and wind direction (Chen et al., 2015; Dankert and Horstmann, 2007; Dankert et al., 2003; Vicen-Bueno et al., 2013), to determine snapshots of the currents at the

80   ocean surface (Senet et al., 2001).

On the basis of these studies and methods a series of commercial oceanographic systems such as WaMoS II (http://www.oceanwaves.de), SeaDarQ (Greenwood et al., 2018) and WaveFinder (Park et al., 2006) were developed. The most widely used system nowadays is WaMoS II (software, hardware and details provided in Reichert at al., 1999) focusing on operational monitoring of the sea state (wind waves and surface currents) and operational management of the oil platforms

85   and ships using nautical X-band radar. In combination with other sources of the data (e.g., altimetric wave radar, vessel hydrodynamic simulator) wind waves estimates from navigational radar can be used in maritime security, for example for the assessment of the ships fatigue due to mechanical environmental influence (Drouet et al., 2013) or for the real-time prediction of the ship motions (Hilmer and Thornhill, 2015).

In this study we present the SeaVision (Fig. 2) system for monitoring of the sea state with navigational marine radar and first

90   data that we collected during three research cruises (Fig. 1). SeaVision is an extension of the system for the sea ice monitoring with navigational marine radar – IceVision (https://ice.vision/en). SeaVision can be used for operational monitoring of the current wind waves' field for individual ships and continuous collection of the wind waves data for building new datasets of the wind waves characteristics in the open ocean. SeaVision was developed in collaboration between Shirshov Institute of Oceanology of the Russian Academy of Sciences (https://ocean.ru/, software for wind waves analysis, marine facilities, data

95   analysis and initiation of the project) and Joint stock company "Marine Complexes and Systems" ("MC&S" J.S.C., https://www.mcs.ru/, hardware, radar signal digitization, data recording and storage). The first version of the SeaVision was tested and validated into two expeditions in the North Atlantic (2020 and 2021) and one expedition in the Arctic (2021, Fig. 1). The major advantage of the collected dataset is that together with collecting data from navigational radar in more than 50

Earth System
Science
Data

Open Access

Discussions

locations in the North Atlantic and Arctic (Fig. 1) we were using Spotter wave buoys simultaneously to directly measure
100   characteristics of the wind waves in the same locations, we also run WaveWatch III (WW3DG) model forced by ERA5
reanalysis (Hersbach et al., 2020) for the period of the research cruises. We present in the study the SeaVision system and
dataset of the measurements of the wind waves in the open ocean and its comprehensive analysis.

In the Section 2 we provide details of expeditions, technical details of the SeaVision and data collection and analysis principles
together with an overview of the WW3 model setup. Section 3 contains analysis and validation of the SeaVision dataset with
105   Spotter buoy and WW3 model output. Concluding remarks are made in the last section.

2 Data collection and analysis principles

2 1 Expeditions
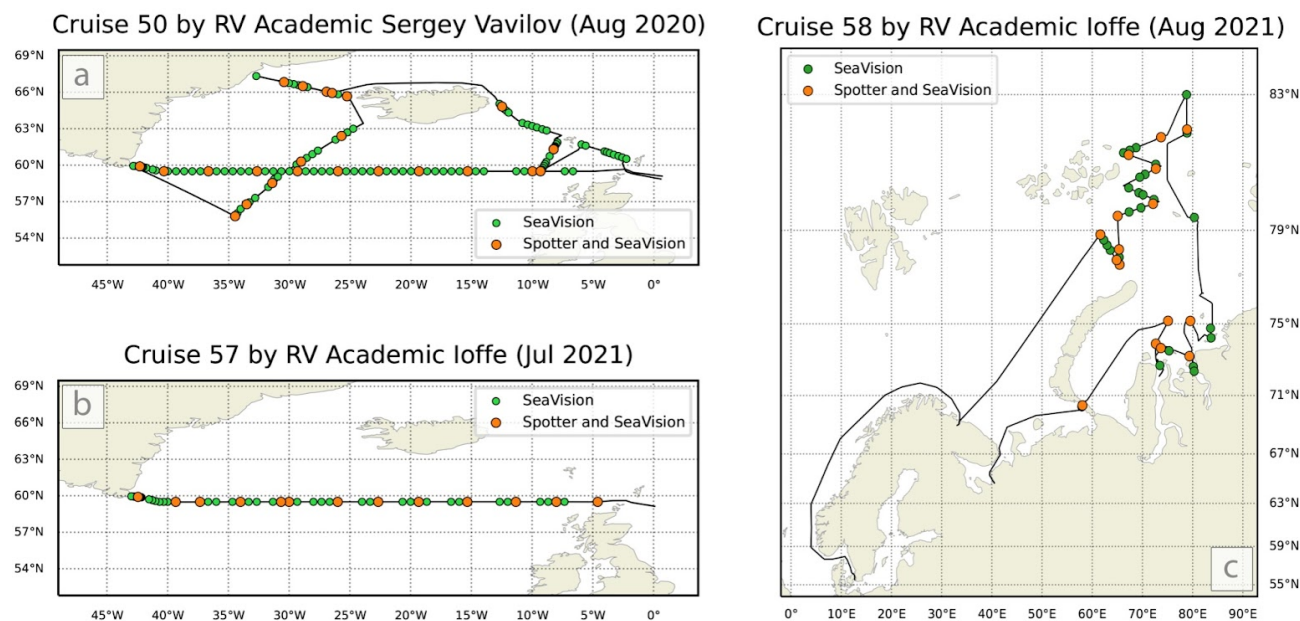
Figure 1: Pathways and dates of the three cruises of the research vessels *Akademic Sergey Vavilov* (a) and *Akademik Ioffe* (b,c). Green dots indicate locations where only SeaVision radar data was collected, orange dots correspond to simultaneous wind waves observations with Spotter wave buoy and SeaVision.

Figure 1 demonstrates pathways and dates of three research cruises, where the wind waves data were collected along with
115   other regular deep ocean observations. All three cruises were carried out by Shirshov Institute of Oceanology of the Russian
Academy of Sciences (IO RAS) within the governmental program of regular ocean observations. In particular, two cruises in

the North Atlantic (Figure 1a,b) are related to regular deep ocean observations at the 59,5°N (Verezemskaya et al., 2021; Falina et al. 2007; Gladyshev et al. 2018, 2019; Sarafanov et al. 2008, 2018) and the Arctic expedition is a part of the IO RAS "Floating University of IORAS" program (Stepanova, 2018). In addition to the regular deep ocean observations in these cruises we were collecting data from navigational radar with the newly developed SeaVision system and simultaneously carrying out observations with Spotter buoy (https://www.sofarocean.com/products/spotter). During all "stations" research vessels were drifting during wave data collection (from 30 minutes to 2 hours) with its engines in neutral position to provide conditions for Spotter buoy wave observations in the free floating mode.

2 2 SeaVision system

2 2 1 Radar signal preprocessing

The first step before actual analysis of the images of the sea clutter is digitization of the radar signal and collection of the images' dataset. Research vessels *Academic Sergey Vavilov* (r/v *ASV*) and *Akademik Ioffe* (r/v *AI*) equipped with standardly operated X-band radar JRC JMA-9110-6XA and JMA-9122-6XA. Technical details of the radars transmission and reception characteristics are given in Table 1. Both radars have 9.41 GHz frequency (radio wavelength ~3 cm), a 6 feet antenna with the horizontal directional resolution of 1.2° (Table 1). Radars have the choice of the pulse lengths: 0.08 µs, 0.25 µs, 0.5 µs, 0.8 µs, 1.0 µs. For our purposes we used the shortest possible pulse length of 0.08 µs (at so-called "short-pulse" mode - SP1), that is equivalent to a 12 m angular spatial resolution.

SeaVision system (Fig. 2) connected to the radar via splitter, it digitizes and records directionally stabilized (northward) radar sea clutter images (converted to netcdf format during postprocessing) of each radar antenna rotation in digital format to the external storage, it is also connected to the ship's navigational equipment and records parameters such as: GPS geographical coordinates, speed of the ground (SOG), course of the ground (COG). Each antenna turn results in a separate ASCII file (~16 MB) with the 4096x4096 matrix (1.875 m discretization at 4096 beam directions) with the sea clutter digitized image, that contains GPS, SOG and COG in the header.

Table 1: JRC JMA-9110-6XA radar (*r/v ASV*) and JMA-9122-6XA (*r/v AI*) transmission and reception characteristics.

Research vessel	*Akademik Sergey Vavilov*	*Akademik Ioffe*
Radar type	JRC JMA-9110-6XA	JMA-9122-6XA
Radar frequency/Wave length	9.41 Ghz / 3.18 cm	9.41 Ghz / 3.18 cm

Earth System
Science
Data

Open Access

Discussions

Antenna rotation speed	27 rpm	24 rpm
Impulse power	10 kW	25 kW
Antenna size	6 ft	6 ft
Pulse length mode	0.08 μs (short pulse)	0.07 μs (short pulse)
Analog-digital converter (ADC) frequency/size of output matrix for one antenna turn	80 Mhz / 4096x4096	80 Mhz / 4096x4096
Azimuthal coverage/resolution	0 – 360°/1.2°	0 – 360°/1.2°
Distance range	231,5 – 2778 m	231,5 – 2778 m
Range resolution	12 m	10.5 m
Analog-digital converter (ADC) frequency/size of output matrix for one antenna turn	80 Mhz / 4096x4096	80 Mhz / 4096x4096
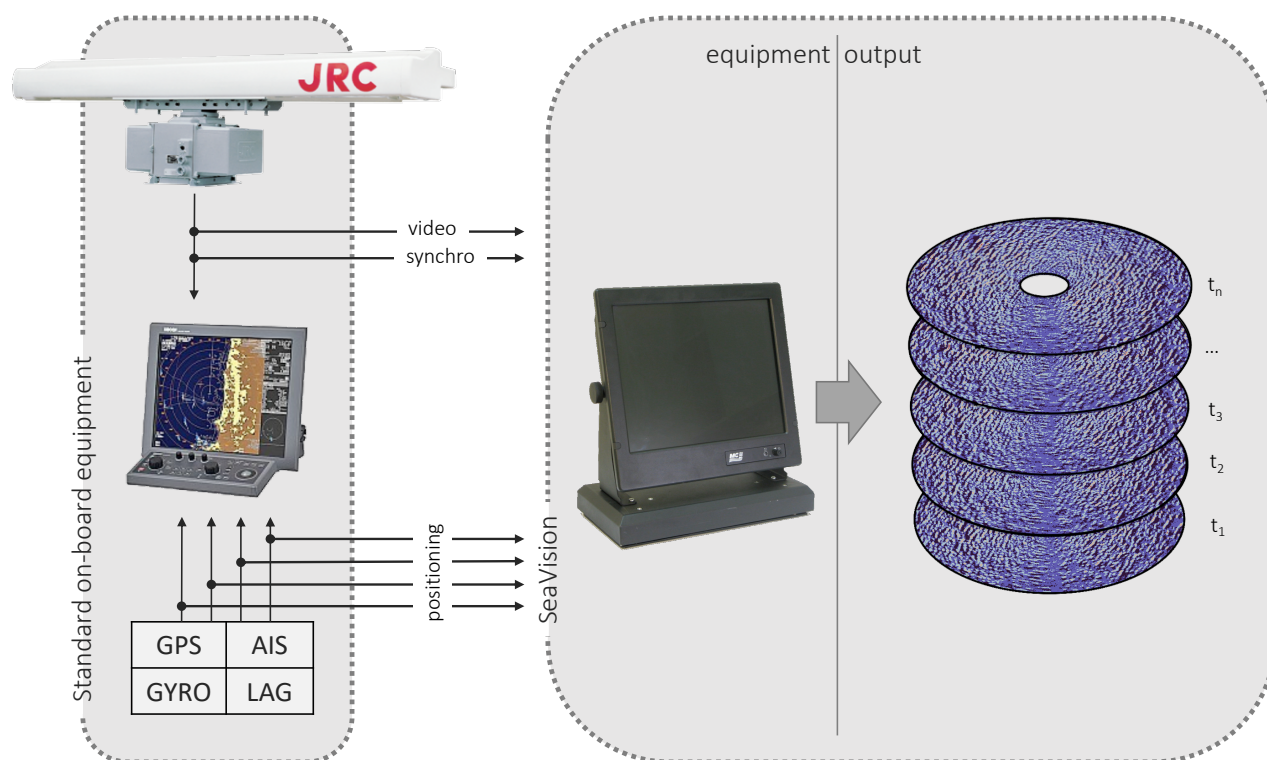
Figure 2: SeaVision integration to the ship's navigational equipment together with an example of the series of the geographically stabilized (northward) sea clutter images, one for each antenna turn (rightest column). Image of the JRC radar scanner (tor left) is taken from the www.jrc.co.jp.

150 **2 2 2 Analysis of the sea clutter images**

For every station (Fig.1) dataset consists of 20 minutes long observations with SeaVision, it is equivalent to a minimum 540 images of the sea clutter (27 antenna turns per minute for JRC JMA-9110-6XA radar) at one station.

Methodology for wind waves' characteristics estimates is a well established FFT-based technique (Nieto-Borge and Guedes
155 Soares, 2000; Borge et al., 2004, Borge et al., 2008 among others). For each station preprocessing of the data begins from the choice of the processing squared area (with a side of 720 m). At this stage we locate the processing area by visual choice of the most apparent wave signal on the images and minimal distance from the ship of 300 m (to avoid potential impact of the ship to the wave field and illumination of the radar signal by the ship). After choosing the area we create the dataset for the further analysis by sampling the same squares from each image (one antenna turn). Data sampled in the polar coordinates were
160 regridded to the Cartesian grid resulting in 384x384 pixels dataset array (with 1.875 m spatial resolution) for each station.

The sequence of these images is then transformed to the 3D spectral domain using fast Fourier transform (FFT, Fig. 3), this results into the three-dimensional spectrum $S(k_x, k_y, f)$, where $f = \omega/2\pi$ is the frequency and ω is the angular

Earth System
Science
Data
Open Access
Discussions

frequency. Further we analyse resulting 3D spectra and extract the part of it that satisfies the linear dispersion relation for ocean waves (Fig. 3): $\Omega = \sqrt{gk\tanh(kH)}$, where k is the wave number absolute value (rad/m), g is the gravity acceleration

165 (m•s^{-1}) and H is significant wave height. Components of the spectra that lie outside of the dispersion relation are assumed to be noise or the signal (Ω_{BGN}), related to the other processes or speckle-noise (Kanevsky, 2008). These spectra estimates are calculated for 16 sectors (with 22.5° width) to get the directional spectra estimates.
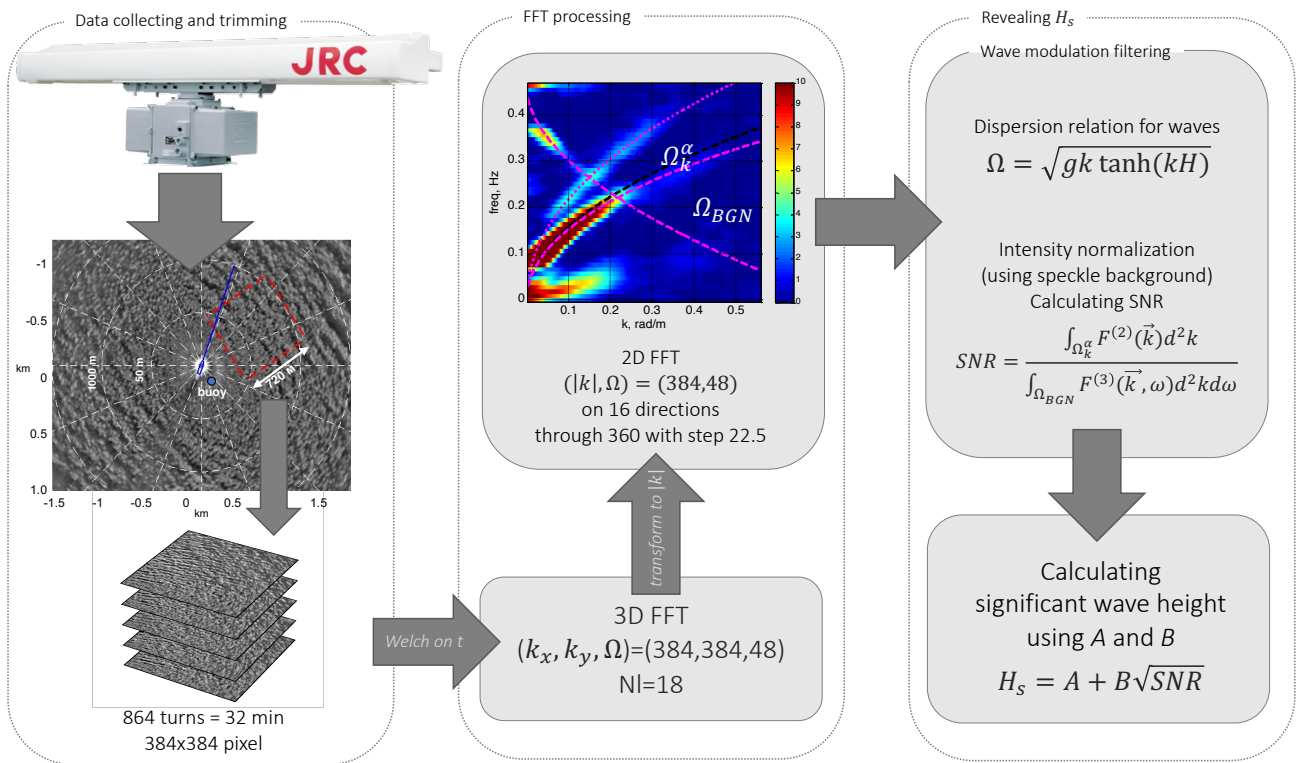
170 **Figure 3: Data processing schematic for estimation of the wind waves parameters from the sea clutter images. Image of the JRC radar scanner (tor left) is taken from the www.jrc.co.jp.**

According to (Nieto-Borge et al., 1999; Hessner et al., 2002; Young et al 1985, Nieto-Borge and Guedes Soares 2000, Ivonin et al. 2016 and others) estimates of the spectra from analysis of the raw radar images reflect spectrum of the radar

175 backscatter rather than actual elevations of the ocean surface due to waves. To convert this spectra to estimates to the wind waves spectra we use a transfer function, so-called signal-to-noise (*SNR*) ratio, where signal is the spectra power that satisfies dispersion relation (Fig. 3) and assumed to be due to the signal, modulated by wind waves, and noise is the remaining signal (spectral power) outside the dispersion relation. Then, according to (Nieto-Borge et al., 1999, 2004) *SNR* can be converted to wave heights with linear regression equation:

180
$$H_s = A + B \sqrt{SNR} \tag{1}$$

where A and B are empirical calibration coefficients individual for each radar. In this study calibration coefficients were calculated on the basis of the simultaneous observations with the Spotter wave buoy (see Section 2.3). Calibration coefficients are also used for calculation of the wave energy spectrum. We also use modulation transfer function (MTF, Nieto-Borge et al.,

185 2004) to correct radar antenna effects of tilting and shadowing to correct the wave energy spectral density. Finally, wave period T_s estimated traditionally using the first moment of the spectrum.

2 3 Spotter wave buoy data

190 To calibrate and validate SeaVision waves observations we performed a series of simultaneous measurements of the wave parameters with Spotter wave buoy (https://www.sofarocean.com/products/spotter). Figure 1 demonstrates the track of the three cruises indicating locations where wind waves were measured simultaneously with Spotter wave buoy and SeaVision, Table A1 provides a list of all locations where SeaVision+Spotter buoy (or SeaVision only) measurements were carried out.

Once the ship was in a drift at the location of the measurements according to the plan of the cruise, the Spotter buoy was

195 equipped, sent overboard and allowed to move away from the ship for at least 200m (as the ship drift is faster than buoy drift due to the local winds, the distance between buoy and ship was constantly increasing). Starting from at least 200m separation the buoy was in a "free floating" mode recording horizontal and vertical displacements of itself. For each station we allowed for at least 20 minutes of the free floating buoy measurements, however at some stations this was up to 1.5 hours. For the homogeneity of the analysis for all stations we use 20-minute time series for wave parameters calculation.

200 Analysis of the raw vertical and horizontal displacements recorded by buoy starts from the selecting in timeseries the "free floating" measurements and further calculation of the significant wave height, wave spectra and directional moments (Fig. 4) using common definitions (see Appendix in Raghukumar et al., 2019), $H_s = 4\sqrt{E}$, where $E = \int_{0.05\,Hz}^{0.3\,Hz} E(f)df$ - the surface elevations variance in the frequency range of the wind waves. More details on calculation of the mean wave direction, directional spread, wave directional spectrum and other parameters on the basis of the Spotter time series can be found in

205 (Raghukumar et al., 2019), together with evaluation of the buoy ability for wave characteristics measurements.

We further use wave parameters derived from buoy as the "ground truth" for the SeaVision calibration and estimation of the radar calibration coefficients A and B, these coefficients are further used to rescale SeaVision wave energy spectrum to match buoy spectrum with least squares.
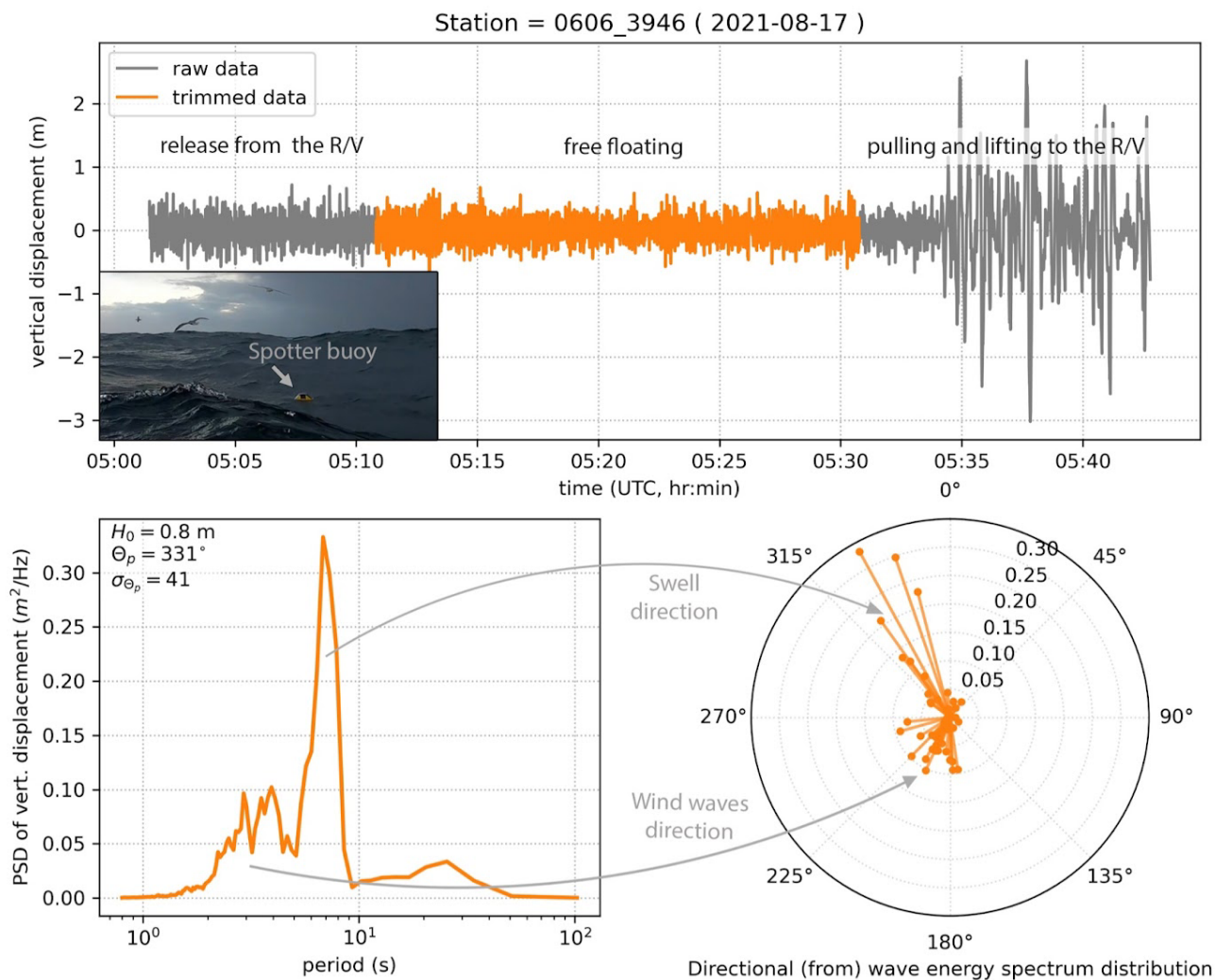
Figure 4: **Spotter wave buoy timeseries of vertical displacements at the station #3946 in the 58th cruise of R/V** *Academic Ioffe* **(top), wave energy spectrum together with significant wave height (bottom left) and directional wave spectrum (bottom right).**

2 4 Meteorological data

Along all cruises the AIRMAR WeatherStation 220WX was mounted at the height of 30m on the mainmast to avoid the impact of the ship on the local meteorology. Weather station provides standard output parameters: barometric pressure, wind speed

10

and direction, air temperature and relative humidity. Wind characteristics were recalculated from apparent wind to true wind in real-time.

220

2 5 WaveWatch III model experiment

Another potential source of the wind waves data in the open ocean is spectral wave modelling. We run WaveWatch III (WW3DG, version 6.07, WW3) spectral wave model with ERA5 reanalysis (Hersbach et al., 2020) as lateral boundary

225 conditions with 0.1° spatial and 1 hourly temporal resolutions. The experiments have been developed to reconstruct two-dimensional wave spectra comparable with SeaVision and Spotter buoy observations. Start and end dates of the experiments were collocated in time with dates of the research cruises. For wave energy input and dissipation we use ST6 parameterization (Bababin, 2006; Bababin, 2011; Rogers et al., 2012; Zieger et al., 2015) and the discrete interaction approximation (DIA) scheme for nonlinear wave interactions (Hasselmann and Hasselmann 1985).

230

3 Validation and overall SeaVision performance

Most of the analyses presented in this section are based on a common source location of surface wave observations from SeaVision, Spotter buoy and WW3 output information.

235 The overall agreement in significant wave height (H_s) estimates is demonstrated in Fig. 5 where we plot difference in H_s estimates: Spotter minus SeaVision (Fig. 5a) and Spotter minus WW3 (Fig, 5b) as a function of wind speed (wind speed recorded by the weather station) for all stations (Table A1). On average WW3 underestimates H_s by 27 cm, while SeaVision on average implies agreement with Spotter buoy data (only 3 cm difference on average). In general, for the lower wind speeds SeaVision underestimates H_s by up to 50 cm and overestimates H_s for the higher wind speeds. This effect can be due to better

240 ripples development on the ocean surface during higher winds affecting the signal to noise ratio (Formula 1).
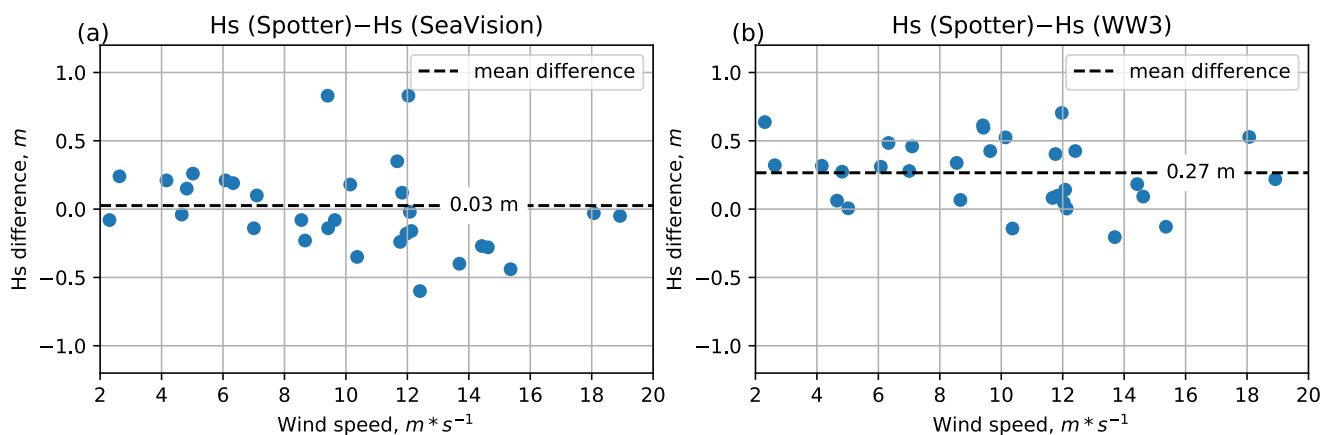
Figure 5: Difference in the significant wave height (H_s) estimates for all stations as function of the wind speed: Spotter buoy ("ground truth") *minus* SeaVision (left panel), Spotter buoy *minus* WW3 (right panel). Dashed line marks mean difference among all stations.

245

At the same time there are two stations (2901 and 2937 see Table A1) where this difference reaches almost 100 cm (between 9 and 12 m/s winds), examinations of weather conditions at these stations revealed that there were not any special weather conditions and observations were carried for H_s between 1.5 and 2 m, however there was a strong drift of the vessel due to the

250 local current that potentially influenced the angles of electromagnetic signal reflection from the surface. Further examination and methodology adjustment required together with more data collection during different conditions in the open ocean are required to investigate into these differences.

Scatterplots for the H_s and wave period (T_s) also demonstrate better agreements between SeaVision and Spotter than between WW3 and Spotter (Fig. 6). Regression coefficients for SeaVision are 0.98 for H_s and 0.9 for T_s and only 0.88 and 0.63 for

255 WW3. There is also no evident dependance for H_s and T_s better or worser agreement between datasets from the amplitude of the H_s and T_s itself. Figure 6 illustrates the accuracy of SeaVision measurements and its performance in sea states up to 4.2 m in significant wave height and 10 s in mean period. There is no obvious difference in the distribution of points for the Spotter-SeaVision in range 0.8 - 3 m of wave heights. SeaVision has a tendency (relatively to buoy) to overestimate mean period. WW3 model mostly underestimates wave heights and periods.
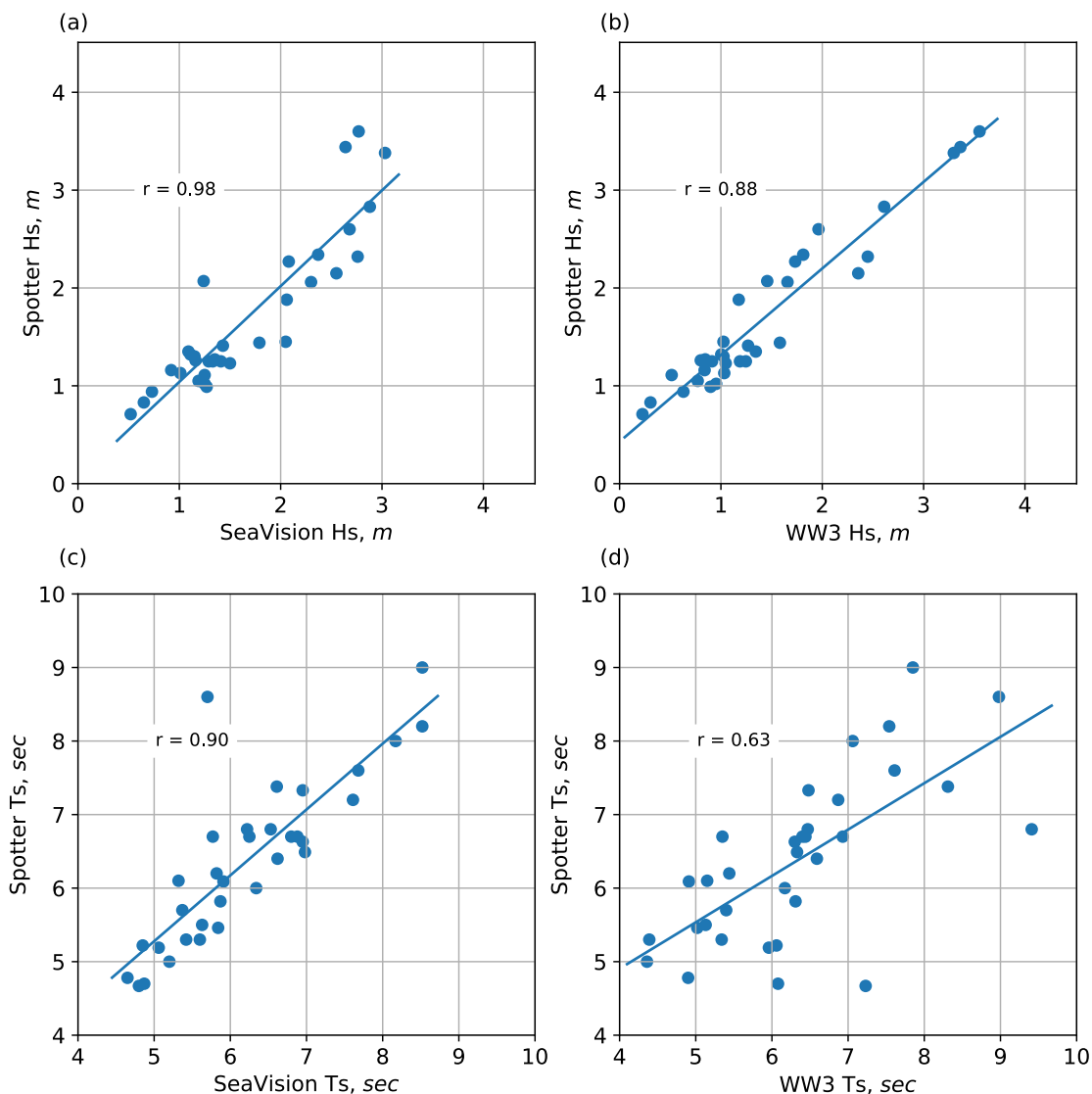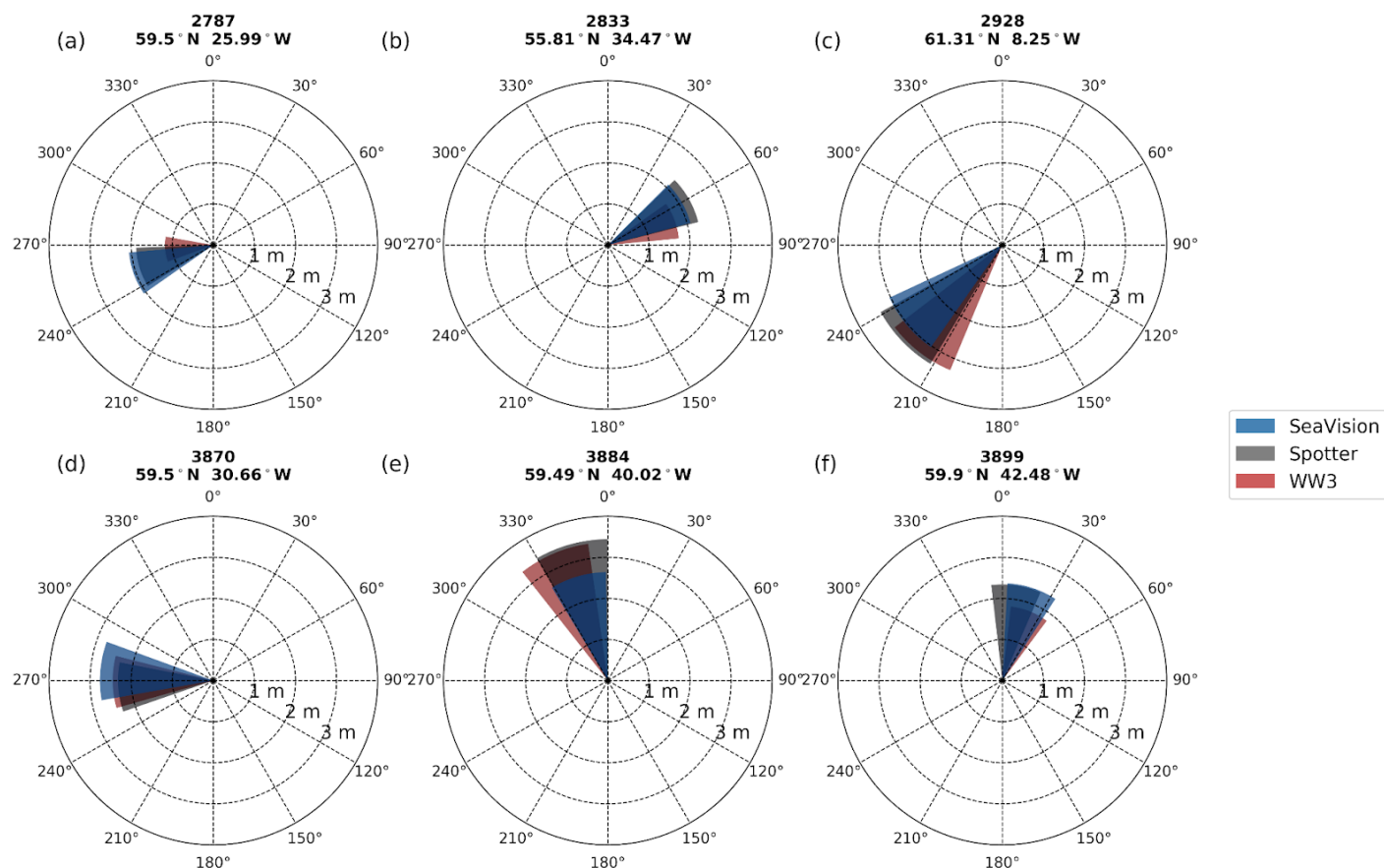
Figure 6: Scatterplots of the significant wave height (H$_s$) and wave period (T$_s$) estimates between SeaVision and Spotter (a,c) and between WW3 and Spotter (b,d) for all stations together with regression coefficients r.

Estimates of the H$_s$ from directional spectra are shown in Figure 7 for six stations (see Table A1). It is important to notice that all three sources of the data: SeaVision, Spotter buoy and WW3 demonstrate higher agreement in estimates of the waves direction (from) than in H$_s$ or T$_s$. The difference in waves direction doesn't exceed 10°.

Figure 7: Diagrams (roses) of wave direction (from) and H$_s$ on the basis of the three data sources: SeaVision (blue), Spotter (gray) and WW3 (red) at the stations: #2787, #2833, #2928, #3870, #3884, #3899 (see Table A1).

Conclusions

In this study we present the dataset of the observations of the wind waves collected during three research cruises (two in the North Atlantic and on in the Arctic) on the basis of usage navigational X-band marine radar and wave buoy Spotter. Nowadays there is still exists gap in the *in situ* observational network for the wind waves, at the same time winds waves is crucially important dynamical component of the interaction between the ocean and the atmosphere and play important role into the climate system. We also present a newly developed SeaVision system for digitizing and recording of the analogous marine radar signal and further analysis of the data to obtain wind waves' parameters such as significant wave height, wave period and wave energy spectra. The potential usage of the dataset is validation of the satellite missions and outputs from the models.

14

Open Access Earth System Science Data Discussions

285   We demonstrate an overall agreement of the estimates of significant wave height and wave period on the basis of SeaVision with the same estimates simultaneously measured by the wave buoy Spotter and modelled by WW3 spectral wave model. At the same time estimates of the significant wave height between WW3, Spotter and SeaVision are in a better agreement than estimates of the wave period. Within the H_s up to 4.2 m and T_s up to 10 s the average difference between SeaVision and Spotter buoy is 3 cm for H_s, while for the Spotter minus WW3 this difference is 27 cm. SeaVision has a tendency (relatively to Spotter) to overestimate mean period by 0.5 s while WW3 both overestimate and underestimate wave periods by up to 2,5 s (regression

290   coefficient with Spotter is only 0.63, Fig. 6). The best agreement among three sources of the data is in estimation of wave directions (Fig. 7), the difference doesn't exceed 10°.

It is important to notice while this paper describes the first results and prime data obtained with SeaVision, the commercial oceanographic systems for the wind waves monitoring such as WaMoS II (http://www.oceanwaves.de), SeaDarQ (http://www.seadarq.com/) and WaveFinder (Park et al., 2006) already exist and successfully operating and providing with

295   wind waves and currents observations. However, our main aim is to develop in the nearest future a low cost, independently operating and stable system that would allow to broaden observational network for the wind waves. Given that all ships navigating into the open ocean are equipped with navigational marine radar the in *situ* observational network for the wind waves can be potentially broaden by installing the low cost and independently operating version of the SeaVision (or any other system) to the Voluntary Observing Ships or to the any ship that would be willing to participate in the wind waves data

300   collection in the open ocean.

Data availability

305   Dataset that contains significant wave height, wave period, wave energy frequency spectrum from both SeaVision and Spotter buoy at the locations of every station (Table A1) is available through the temporary link (https://sail.ocean.ru/tilinina2021/) while supporting dataset (Tilinina et al., 2021) is in technical processing at PANGAEA repository. Users interested in the analysis of the raw radar dataset are welcome to request access from Alexander Gavrikov (gavr@sail.msk.ru).

310   **Appendix A: List of the locations (stations) of the wind waves measurements during three research cruises**
Table A1: Stations list: geographical locations and time of all stations where the wind waves measurements were performed simultaneously with SeaVision and Spotter buoy.

#	Station #	Start UTC time	End UTC time	Latitude° N	Longitude° E	Cruise #

1	**2868**	27.08.2020 13:53	27.08.2020 14:13	65.67	-25.26	ASV50
2	**2881**	28.08.2020 10:45	28.08.2020 11:05	66.49	-28.89	ASV50
3	**2885**	28.08.2020 19:05	28.08.2020 19:25	66.84	-30.43	ASV50
4	**2763**	11.08.2020 11:25	11.08.2020 11:45	59.50	-10.00	ASV50
5	**2771**	12.08.2020 17:00	12.08.2020 17:20	59.50	-15.33	ASV50
6	**2777**	13.08.2020 18:15	13.08.2020 18:35	59.50	-19.32	ASV50
7	**2782**	14.08.2020 18:42	14.08.2020 19:02	59.50	-22.66	ASV50
8	**2787**	15.08.2020 18:10	15.08.2020 18:30	59.50	-25.99	ASV50
9	**2792**	16.08.2020 14:45	16.08.2020 15:05	59.50	-29.33	ASV50
10	**2797**	17.08.2020 10:12	17.08.2020 10:32	59.50	-32.67	ASV50
11	**2803**	18.08.2020 12:17	18.08.2020 12:37	59.50	-36.67	ASV50
12	**2809**	19.08.2020 13:26	19.08.2020 13:46	59.50	-40.34	ASV50
13	**2821**	20.08.2020 13:44	20.08.2020 14:04	59.90	-42.32	ASV50
14	**2833**	22.08.2020 15:26	22.08.2020 15:46	55.81	-34.47	ASV50
15	**2841**	23.08.2020 12:31	23.08.2020 12:51	56.78	-33.53	ASV50

16	2849	24.08.2020 14:06	24.08.2020 14:26	58.53	-31.43	ASV50
17	2856	25.08.2020 12:42	25.08.2020 13:02	60.30	-29.04	ASV50
18	2863	26.08.2020 11:45	26.08.2020 12:05	62.40	-25.73	ASV50
19	2901	30.08.2020 13:05	30.08.2020 13:25	65.94	-26.49	ASV50
20	2903	01.09.2020 13:05	01.09.2020 13:25	64.82	-12.49	ASV50
21	2928	03.09.2020 19:24	03.09.2020 19:44	61.31	-8.25	ASV50
22	2937	04.09.2020 21:16	04.09.2020 21:36	59.50	-9.31	ASV50
23	3831	29.06.2021 19:49	29.06.2021 20:09	59.50	-4.60	AI57
24	3836	30.06.2021 12:50	30.06.2021 13:10	59.50	-8.00	AI57
25	3841	01.07.2021 09:26	01.07.2021 09:46	59.49	-11.33	AI57
26	3847	02.07.2021 10:33	02.07.2021 10:53	59.50	-15.33	AI57
27	3853	03.07.2021 12:35	03.07.2021 12:55	59.50	-19.33	AI57
28	3858	04.07.2021 11:38	04.07.2021 11:58	59.50	-22.67	AI57
29	3863	05.07.2021 10:05	05.07.2021 10:25	59.50	-26.00	AI57
30	3870	06.07.2021 16:29	06.07.2021 16:49	59.50	-30.67	AI57

31	3875	07.07.2021 15:57	07.07.2021 16:17	59.52	-33.98	AI57
32	3880	08.07.2021 17:32	08.07.2021 17:52	59.50	-37.33	AI57
33	3884	09.07.2021 13:51	09.07.2021 14:11	59.50	-40.00	AI57
34	3899	11.07.2021 12:45	11.07.2021 13:05	59.90	-42.48	AI57
35	3911	12.08.2021 13:27	12.08.2021 13:47	70.37	58.04	AI58
36	3929	14.08.2021 21:43	14.08.2021 22:03	75.15	75.09	AI58
37	3930	15.08.2021 06:40	15.08.2021 07:00	73.98	72.66	AI58
38	3939	16.08.2021 12:40	16.08.2021 13:00	73.75	73.66	AI58
39	3946	17.08.2021 04:53	17.08.2021 05:13	73.31	79.35	AI58
40	3956	18.08.2021 12:52	18.08.2021 13:12	75.14	79.54	AI58
41	3972	21.08.2021 12:27	21.08.2021 12:47	82.14	78.88	AI58
42	3982	22.08.2021 15:48	22.08.2021 16:08	81.93	73.70	AI58
43	3990	23.08.2021 14:43	23.08.2021 15:03	81.44	67.25	AI58
44	3997	24.08.2021 08:02	24.08.2021 08:22	81.04	72.66	AI58
45	4013	25.08.2021 19:28	25.08.2021 19:48	79.93	72.11	AI58

18

46	4020	26.08.2021 13:20	26.08.2021 13:40	79.51	65.06	AI58
47	4025	27.08.2021 03:05	27.08.2021 03:25	78.28	65.33	AI58
48	4029	27.08.2021 12:39	27.08.2021 12:59	77.67	65.45	AI58
49	4031	27.08.2021 18:30	27.08.2021 18:50	77.86	64.85	AI58
50	4040	28.08.2021 11:11	28.08.2021 11:31	78.84	61.62	AI58

315

Author contributions

NT, AG, DI, VS, AS, LS, VS and PS participated in research cruises and data collection. The leading role in field work program development and implementation belongs to AG and VS. DI made preprocessing, postprocessing and analysis of the radar

320 (SeaVision) dataset, VS developed configuration and run WW3 model for the period of cruises, AG analysed all Spotter buoy data. VF, BT and SB provided hardware development and mounting of the SeaVision to the research vessels. NT has a leading role in the project set up and manuscript writing. The initial idea of the research belongs to SG. All authors contributed to the discussion, interpretation of the results and writing.

325 **Competing interests**

The authors declare no conflict of interests.

Acknowledgements

330

335

Financial support

19

Earth System
Open Access
Science
Data
Discussions

References

Borge, J. C. N., Reichert, K. and Dittmer, J.: Use of nautical radar as a wave monitoring instrument, Coastal Engineering,
345   37(3–4), https://doi.org/10.1016/S0378-3839(99)00032-0,1999.

Buckley, J. R. and Aler, J.: Estimation of ocean wave height from grazing incidence microwave backscatter, in International Geoscience and Remote Sensing Symposium (IGARSS),vol. 2., https://doi.org/10.1109/IGARSS.1997.615328, 1997.

350   Buckley, J. R. and Aler, J.: Enhancements in the determination of ocean surface wave height from grazing incidence microwave backscatter, in International Geoscience and Remote Sensing Symposium (IGARSS), vol.5.,https://doi.org/10.1109/IGARSS.1998.702254, 1998.

Campana, J., Terrill, E. J. and Paolo, T. de: A new inversion method to obtain upper-ocean current-depth profiles using X-
355   band observations of deep-water waves, Journal of Atmospheric and Oceanic Technology, 34(5), https://doi.org/10.1175/JTECH-D-16-0120.1, 2017.

Cavaleri, L., Barbariol, F. and Benetazzo, A.: Wind-wave modeling: Where we are, where to go, Journal of Marine Science and Engineering, 8(4), https://doi.org/10.3390/JMSE8040260, 2020.
360
Chen, Z., He, Y., Zhang, B., & Qiu, Z. (2015). Determination of nearshore sea surface wind vector from marine X-band radar images. *Ocean Engineering*, *96*, 79–85,https://doi.org/10.1016/J.OCEANENG.2014.12.019, 2015.

Chen, Z., Zhang, B., Kudryavtsev, V., He, Y., & Chu, X. (2019). Estimation of sea surface current from X-band marine radar
365   images by cross-spectrum analysis. *Remote Sensing*, *11*(9), https://doi.org/10.3390/rs11091031, 2019.

Crombie, D. D.: Doppler spectrum of sea echo at 13.56 Mc./s. [3], Nature, 175(4459), https://doi.org/10.1038/175681a0, 1955.

Dankert, H., Horstmann, J. and Rosenthal, W.: Ocean wind fields retrieved from radar-image sequences, Journal of
370   Geophysical Research: Oceans, 108(11), https://doi.org/10.1029/2003jc002056, 2003.

Dankert, H. and Horstmann, J.: A marine radar wind sensor, Journal of Atmospheric and Oceanic Technology, 24(9), https://doi.org/10.1175/JTECH2083.1, 2007.

375   Derkani, M. H., Alberello, A., Nelli, F., Bennetts, L. G., Hessner, K. G., Machutchon, K., Reichert, K., Aouf, L., Khan, S. and Toffoli, A.: Wind, waves, and surface currents in the Southern Ocean: Observations from the Antarctic Circumnavigation Expedition, Earth System Science Data, 13(3), https://doi.org/10.5194/essd-13-1189-2021, 2021.

Drazen, D., Terrill, E., Walker, D., Hazard, J., Cook, T. and Scott, S.: Full-scale measurements of wave impact loading on a
380 flat plate, in Proceedings of the International Conference on Offshore Mechanics and Arctic Engineering - OMAE, vol. 1, Rio
de Janeiro, Brazil, 1–6 July 2012, OMAE2012-83608, https://doi.org/10.1115/OMAE2012-83608, 2012.

Drouet, C., Cellier, N., Raymond, J. and Martigny, D.: Sea state estimation based on ship motions measurements and data
fusion, in Proceedings of the International Conference on Offshore Mechanics and Arctic Engineering - OMAE, vol. 5., Nantes,
385 France, 9–14 June 2013, OMAE2013-10657, https://doi.org/10.1115/OMAE2013-10657, 2013.

Rogers, W. E., Babanin, A. V. and Wang, D. W.: Observation-consistent input and whitecapping dissipation in a model for
wind-generated surface waves: Description and simple calculations, Journal of Atmospheric and Oceanic Technology, 29(9),
https://doi.org/10.1175/JTECH-D-11-00092.1, 2012.
390

Falina, A., Sokov, A., & Sarafanov, A.: Variability and renewal of Labrador Sea Water in the Irminger basin in 1991–2004.
Journal of Geophysical Research, 112, C01006. https://doi.org/10.1029/2005JC003348, 2007.

Fujii, S., Heron, M. L., Kim, K., Lai, J. W., Lee, S. H., Wu, X., Wu, X., Wyatt, L. R. and Yang, W. C.: An overview of
395 developments and applications of oceanographic radar networks in Asia and Oceania countries, Ocean Science Journal, 48(1),
https://doi.org/10.1007/s12601-013-0007-0, 2013.

Gangeskar, R.: Adaptive method for estimation of wave height based on statistics of sea surface images, in International
Geoscience and Remote Sensing Symposium (IGARSS), vol. 1., https://doi.org/10.1109/IGARSS.2000.860484, 2000.
400

Gangeskar, R.: Wave height derived by texture analysis of X-band radar sea surface images, in International Geoscience and
Remote Sensing Symposium (IGARSS), vol. 7., https://doi.org/10.1109/IGARSS.2000.860301, 2000.

Gavrikov, A., Gulev, S. K., Markina, M., Tilinina, N., Verezemskaya, P., Barnier, B., Dufour, A., Zolina, O., Zyulyaeva, Y.,
405 Krinitskiy, M., Okhlopkov, I. and Sokov, A.: RAS-NAAD: 40-yr high-resolution north atlantic atmospheric hindcast for
multipurpose applications (new dataset for the regional mesoscale studies in the atmosphere and the ocean), Journal of Applied
Meteorology and Climatology, 59(5), https://doi.org/10.1175/JAMC-D-19-0190.1, 2020.

Gladyshev, S. V., Gladyshev, V. S., Gulev, S. K., & Sokov, A. V.: Structure and variability of the meridional overturning
410 circulation in the North Atlantic subpolar gyre, 2007–2017. Doklady Earth Sciences, 483(2), 1524–1527.
https://doi.org/10.1134/S1028334X18120024, 2018.

Gladyshev, S. V., Gladyshev, V. S., Klyuvitkin, A. A., & Gulev, S. K.: A new look at the water exchange between the arctic
and the north Atlantic in the Iceland Basin. Doklady Earth Sciences, 485(2), 401–404.
415 https://doi.org/10.1134/S1028334X19040020, 2019.

Greenwood C., Vogler A., Morrison J., Murray A.: The approximation of a sea surface using a shore mounted X-band radar
with low grazing angle. Remote Sensing of Environment, 204, 439-447, https://doi.org/10.1016/j.rse.2017.10.012, 2018.

420 Hasselmann, K.: Theory of synthetic aperture radar ocean imaging: a MARSEN view., Journal of Geophysical Research,
90(C3), https://doi.org/10.1029/JC090iC03p04659, 1985.

Hasselmann, K., Hasselmann, S., Bauer, E., Janssen, P. A. E. M., Komen, G. J., Bertotti, L., Lionello, P., Guillaume, A.,
Cardone, V. C., Greenwood, J. A., Reistad, M., Zambresky, L. and Ewing, J. A.: The WAM model - a third generation ocean
425 wave prediction model., J. PHYS. OCEANOGR., 18(12, Dec. 1988), https://doi.org/10.1175/1520-
0485(1988)018<1775:TWMTGO>2.0.CO;2, 1988.

Hasselmann, S., Hasselmann, K., Allender, J. H. and Barnett, T. P.: Computations and parameterizations of the nonlinear energy transfer in a gravity-wave spectrum. Part II: parameterizations of the nonlinear energy transfer for application in wave
430 models., J. PHYS. OCEANOGR., 15(11, Nov. 1985), https://doi.org/10.1175/1520-0485(1985)015<1369:CAPOTN>2.0.CO;2, 1985.

Hatten, H., Seemann, J., Horstmann, J. and Ziemer, F.: Azimuthal dependence of the radar cross section and the spectral background noise of a nautical radar at grazing incidence, in International Geoscience and Remote Sensing Symposium
435 (IGARSS), vol. 5.,https://doi.org/10.1109/IGARSS.1998.702255,1998.

Hersbach, H., Bell, B., Berrisford, P., Hirahara, S., Horányi, A., Muñoz-Sabater, J., ... & Thépaut, J. N.: The ERA5 global reanalysis, Quarterly Journal of the Royal Meteorological Society, 146(730), 1999-2049, https://doi.org/10.1002/qj.3803, 2010.
440

Hessner, K. and Hanson, J. L.: Extraction of coastal wavefield properties from X-band radar, in International Geoscience and Remote Sensing Symposium (IGARSS), https://doi.org/10.1109/IGARSS.2010.5650134, 2010.

Hessner, K., Wallbridge, S. and Dolphin, T.: Validation of areal wave and current measurements based on X-band radar, in
445 2015 IEEE/OES 11th Current, Waves and Turbulence Measurement, CWTM 2015., https://doi.org/10.1109/CWTM.2015.7098102, 2015.

Hilmer, T. and Thornhill, E.: Observations of predictive skill for real-time Deterministic Sea Waves from the WaMoS II, in OCEANS 2015 - MTS/IEEE Washington., 2016.
450 Hwang, P. A., Sletten, M. A. and Toporkov, J. V.: A note on Doppler processing of coherent radar backscatter from the water surface: With application to ocean surface wave measurements, Journal of Geophysical Research: Oceans, 115(3), https://doi.org/10.1029/2009JC005870, 2010.

Izquierdo, P., Guedes Soares, C., Nieto-Borge, J. C. and Rodríguez, G. R.: A comparison of sea-state parameters from nautical
455 radar images and buoy data, Ocean Engineering, 31(17–18), https://doi.org/10.1016/j.oceaneng.2004.04.004, 2004.

Johnson, J. T., Burkholder, R. J., Toporkov, J. V., Lyzenga, D. R. and Plant, W. J.: A numerical study of the retrieval of sea surface height profiles from low grazing angle radar data, in IEEE Transactions on Geoscience and Remote Sensing, vol. 47., https://doi.org/10.1109/IGARSS.2010.5650134, 2009.
460

Liu, Q., Rogers, W. E., Babanin, A. V., Young, I. R., Romero, L., Zieger, S., Qiao, F. and Guan, C.: Observation-based source terms in the third-generation wave model WAVEWATCH III: Updates and verification, Journal of Physical Oceanography, 49(2), https://doi.org/10.1175/JPO-D-18-0137.1, 2019.

465 Lund, B., Collins, C. O., Graber, H. C., Terrill, E. and Herbers, T. H. C.: Marine radar ocean wave retrieval's dependency on range and azimuth, in Ocean Dynamics, vol. 64., http://dx.doi.org/10.1007/s10236-014-0725-6, 2014.

Nagai, T., Satomi, S., Terada, Y., Kato, T., Nukada, K. and Kudaka, M.: GPS buoy and seabed installed wave gauge application to offshore tsunami observation, in Proceedings of the International Offshore and Polar Engineering Conference, vol. 2005.,
470 Seoul, Korea, 19–24 June 2005,ISOPE-I-05-282, available at: https://onepetro.org/ISOPEIOPEC/proceedings-abstract/ISOPE05/All-ISOPE05/ISOPE-I-05-282/9448, 2005.

Nieto-Borge, J. C. and Guedes Soares, C.: Analysis of directional wave fields using X-band navigation radar, Coastal Engineering, 40(4), https://doi.org/10.1016/S0378-3839(00)00019-3, 2000.
475 Nieto-Borge, J. C., Hessner, K., Jarabo-Amores, P. and De La Mata-Moya, D.: Signal-to-noise ratio analysis to estimate ocean wave heights from X-band marine radar image time series, IET Radar, Sonar and Navigation, 2(1), https://doi.org/10.1049/iet-rsn:20070027, 2008.

480   Nieto-Borge, J. C., Jarabo-Amores, P., De La Mata-Moya, D. and López-Ferreras, F.: Estimation of ocean wave heights from temporal sequences of X-band marine radar images, in European Signal Processing Conference., Lüneburg, Germany 4–9 June 2006, 35 – 41, https://doi.org/10.1115/OMAE2006-92015, 2006.

Plant, W. J., Keller, W. C., Reeves, A. B., Uliana, E. A. and Johnson, J. W.: Airborne microwave doppler measurements of ocean wave directional spectra, International Journal of Remote Sensing, 8(3), https://doi.org/10.1080/01431168708948644,
485   1987.

Plant, W. J.: A model for microwave Doppler sea return at high incidence angles: Bragg scattering from bound, Tilted waves, Journal of Geophysical Research: Oceans, 102(C9), https://doi.org/10.1029/97JC01225, 1997.

490   Park, G. I., Choi, J. W., Kang, Y. T., Ha, M. K., Jang, H. S., Park, J. S., Kwon, S. H.
(2006). The application of marine X-band radar to measure wave condition during sea trial. Journal of Ship and Ocean Technology, 10(4), 34-48, available at: https://www.koreascience.or.kr/article/JAKO200614539116884.page, 2006.

Raghukumar, K., Chang, G., Spada, F., Jones, C., Janssen, T. and Gans, A.: Performance characteristics of "spotter,"' a newly
495   developed real-time wave measurement buoy, Journal of Atmospheric and Oceanic Technology, 36(6), https://doi.org/10.1175/JTECH-D-18-0151.1, 2019.

Reichert, K., Hessner, K., Dannenberg, J. and Traenkmann, I.: X-Band radar as a tool to determine spectral and single wave properties, in Proceedings of the International Conference on Offshore Mechanics and Arctic Engineering - OMAE, vol. 2006.,
500   Hamburg, Germany, 4–9 June 2006, 683-688, https://doi.org/10.1115/OMAE2006-92015, 2006.

Ribal, A. and Young, I. R.: Publisher Correction: 33 years of globally calibrated wave height and wind speed data based on altimeter observations (Scientific Data, (2019), 6, 1, (77), 10.1038/s41597-019-0083-9), Scientific Data, 6(1), https://doi.org/10.1038/s41597-019-0108-4, 2019.
505
Sarafanov, A., Falina, A., Sokov, A., & Demidov, A.: Intense warming and salinification of intermediate waters of southern origin in the eastern subpolar North Atlantic in the 1990s to mid-2000s. Journal of Geophysical Research, 113(C12). https://doi. org/10.1029/2008JC004975, 2008.

510   Sarafanov, A., Falina, A., Sokov, A., Zapotylko, V., & Gladyshev, S.: Ship-based monitoring of the northern north Atlantic Ocean by the Shirshov Institute of Oceanology. The main results. In Ship based monitoring of the northern North Atlantic ocean by the Shirshov Institute of Oceanology. The Ocean in Motion (pp. 415–427). Springer Oceanography. https://doi.org/10.1007/978-3-319-71934-4_25, 2018.

515   Seemann, J., Senet, C. M., Wolff, U. and Ziemer, F.: Nautical x-band radar image processing: Monitoring of morphodynamic processes in coastal waters, Oceans Conference Record (IEEE), 2, Providence, RI, USA,11-14 September 2000, 1329-1335, https://doi.org/10.1109/OCEANS.2000.881788, 2000.

Seemann, J., Ziemer, F. and Senet, C. M.: Method for computing calibrated ocean wave spectra from measurements with a
520   nautical X-band radar, in Oceans Conference Record (IEEE), vol. 2., Halifax, NS, Canada, 6-9 October 1997, https://doi.org/10.1109/OCEANS.1997.624154, 1997.

Senet, C. M., Seemann, J. and Ziemer, F.: The near-surface current velocity determined from image sequences of the sea surface, IEEE Transactions on Geoscience and Remote Sensing, 39(3), https://doi.org/10.1109/36.911108, 2001.
525

Senet, C. M., Seemann, J., Flampouris, S. and Ziemer, F.: Determination of bathymetric and current maps by the method DiSC based on the analysis of nautical X-band radar image sequences of the sea surface (November 2007), IEEE Transactions on Geoscience and Remote Sensing, 46(8), https://doi.org/10.1109/TGRS.2008.916474, 2008.

530 Shen, C., Huang, W., Gill, E. W., Carrasco, R. and Horstmann, J.: An algorithm for surface current retrieval from X-band marine radar images, Remote Sensing, 7(6), https://doi.org/10.3390/rs70607753, 2015.

Stepanova N.B.: The first scientific school within the educational program "Floating University of IO RAS", Journal of oceanological research, 46(1), 189-191, https://doi.org/10.29006/1564-2291.JOR-2018.46(1).19, 2019.

535

Story, W. R., Fu, T. C. and Hackett, E. E.: Radar measurement of ocean waves, in Proceedings of the International Conference on Offshore Mechanics and Arctic Engineering - OMAE, vol. 6., https://doi.org/10.1115/OMAE2011-49895, 2011.

Sverdrup, H. U. and Munk, W. H.: Wind, Sea, and Swell. Theory of Relations For Forecasting, Office, (601), available at:
540 https://books.google.com/books?id=LxtSAQAAMAAJ&printsec=frontcover&hl=ru&source=gbs_ge_summary_r&cad=0#v=onepage&q&f=false, 1947.

The WAVEWATCH III Development Group (WW3DG), (2019): User manual and system documentation of WAVEWATCH III R version 6.07. Tech. Note 333, NOAA/NWS/NCEP/MMAB, College Park, MD, USA, 465 pp. + Appendices., available
545 at: https://github.com/NOAA-EMC/WW3/wiki/Manual, 2019.

Terrill, E. J.: X-band Observations of Waves, Algorithm Development, and Validation High Resolution Wave-Air-Sea Interaction DRI, ONR Annual Rept. 2009, available at:https://www.google.com/books/edition/X_band_Observations_of_Waves_Algorithm_D/tOauAQAACAAJ?hl=en, 2009.
550

Tilinina N., Ivonin D., Gavrikov A., Sharmar V., Gulev S., Suslov A., Fadeev V., Trofimov B., Bargman S., Salavatova L., Koshkina V., Shishkova P., Sokov A.: Wind waves in the North Atlantic and Arctic from ship navigational radar (SeaVision system) and wave buoy Spotter during three research cruises in 2020 and 2021, PANGAEA, 2021, in technical processing.

555 Swail,V., Jensen, R.E., Lee, B., Turton, J., Thomas, J., Gulev, S., Yelland, M., Etala, P., Meldrum, D., Birkemeier, W., Burnett B. and Warren G.: Wave Measurements, Needs and Developments for the Next Decade., available at: http://waveworkshop.org/11thWaves/Papers/Swail_etal_Wave%20Measurements.pdf, 2010.

Verezemskaya, P., Barnier, B., Gulev, S. K., Gladyshev, S., Molines, J. M., Gladyshev, V., Lellouche, J. M. and Gavrikov,
560 A.: Assessing Eddying (1/12°) Ocean Reanalysis GLORYS12 Using the 14-yr Instrumental Record From 59.5°N Section in the Atlantic, Journal of Geophysical Research: Oceans, 126(6), https://doi.org/10.1029/2020JC016317, 2021.

Vicen-Bueno, R., Horstmann, J., Terril, E., de Paolo, T. and Dannenberg, J.: Real-time ocean wind vector retrieval from marine radar image sequences acquired at grazing angle, Journal of Atmospheric and Oceanic Technology, 30(1),
565 https://doi.org/10.1175/JTECH-D-12-00027.1, 2013.

Vicen-Bueno, R., Lido-Muela, C. and Nieto-Borge, J. C.: Estimate of significant wave height from noncoherent marine radar images by multilayer perceptrons, Eurasip Journal on Advances in Signal Processing, 2012(1), https://doi.org/10.1186/1687-6180-2012-84, 2012.
570

Vogelzang, J., Boogaard, K., Reichert, K. and Hessner, K.: Wave height measurements with navigation radar, International Archives of Photogrammetry and Remote Sensing, 33(B7), available at:https://www.researchgate.net/profile/Jur-Vogelzang/publication/228406388_WAVE_HEIGHT_MEASUREMENTS_WITH_NAVIGATION_RADAR/links/02e7e53ccf36acf893000000/WAVE-HEIGHT-MEASUREMENTS-WITH-NAVIGATION-RADAR.pdf, 2000.

575

Wetzel, L. B.: Electromagnetic Scattering from the Sea at Low Grazing Angles, in Surface Waves and Fluxes.,https://doi.org/10.1007/978-94-009-0627-3_3,1990.

580 Young, I. R., Rosenthal, W. and Ziemer, F.: A three-dimensional analysis of marine radar images for the determination of ocean wave directionality and surface currents., Journal of Geophysical Research, 90(C1), https://doi.org/10.1029/JC090iC01p01049, 1985.

Young, I. R. and Babanin, A. V.: Spectral distribution of energy dissipation of wind-generated waves due to dominant wave breaking, Journal of Physical Oceanography, 36(3), https://doi.org/10.1175/JPO2859.1, 2006.
585